Article

Cite This: *Biomacromolecules* 2018, 19, 364–373

pubs.acs.org/Biomac

Electrical Programming of Soft Matter: Using Temporally Varying Electrical Inputs To Spatially Control Self Assembly

Kun Yan,[†,#,▽] Yi Liu,[‡,§,▽] Jitao Zhang,[§] Santiago O. Correa,[∥] Wu Shang,[§] Cheng-Chieh Tsai,[⊥] William E. Bentley,[‡,§] Jana Shen,[⊥] Giuliano Scarcelli,[§] Christopher B. Raub,[∥] Xiao-Wen Shi,*[,†] and Gregory F. Payne*[,‡,§]

[†]School of Resource and Environmental Science, Hubei International Scientific and Technological Cooperation Base of Sustainable Resource and Energy, Wuhan University, Wuhan 430079, China

[‡]Institute for Bioscience and Biotechnology Research, University of Maryland College Park, College Park, Maryland 20742, United States

[§]Fischell Department of Bioengineering, University of Maryland College Park, College Park, Maryland 20742, United States

[∥]Department of Biomedical Engineering, The Catholic University of America, Washington, D.C. 20064, United States

[⊥]Department of Pharmaceutical Sciences, University of Maryland School of Pharmacy, Baltimore, Maryland 21201, United States

Supporting Information

ABSTRACT: The growing importance of hydrogels in translational medicine has stimulated the development of top-down fabrication methods, yet often these methods lack the capabilities to generate the complex matrix architectures observed in biology. Here we show that temporally varying electrical signals can cue a self-assembling polysaccharide to controllably form a hydrogel with complex internal patterns. Evidence from theory and experiment indicate that internal structure emerges through a subtle interplay between the electrical current that triggers self-assembly and the electrical potential (or electric field) that recruits and appears to orient the polysaccharide chains at the growing gel front. These studies demonstrate that short sequences (minutes) of low-power (~1 V) electrical inputs can provide the program to guide self-assembly that yields hydrogels with stable, complex, and spatially varying structure and properties.

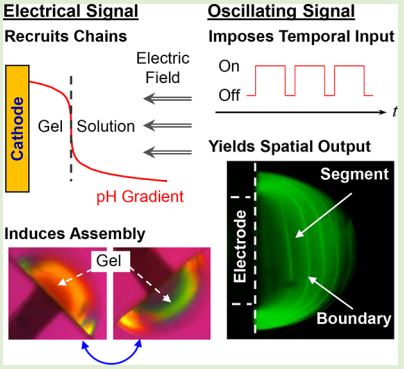

1. INTRODUCTION

The growing importance of hydrogels in biomedical applications[1−3] is stimulating the development of a range of top-down fabrication strategies.[4−7] A major goal for such fabrication methods is to create hydrogels with complex structures[8,9] that can be controlled independently from changes in chemical composition. One motivation for controlling structure is to enable a precise tuning of the mechanical properties that regulate cell behaviors,[10−14] such as cell adhesion and spreading,[15−17] proliferation,[18] and differentiation.[19−21] In addition, precise control of internal structure may allow hydrogels to be created with anisotropic transport properties that confer directionality to the diffusion of cell signaling molecules that can cue development along desired programs.[22−24] Whereas there has been exciting progress in the ability to control hydrogel structure and properties, current top-down methods are still unable to recapitulate the complex internal matrix structure that is characteristic of biology.

Biology's ability to generate complex matrices serves as an inspiration for the programmable construction of soft matter.[25,26] In many cases biology uses diffusible chemical cues (i.e., morphogens[27,28]) to create spatial patterns, while reaction-diffusion models are often invoked to provide a framework[29,30] to understand such patterning.[31−35] As illustrated in Scheme 1a, a classic example is the clock and wavefront model used to explain the emergence of the segmented structure of embryonic somites.[36,37] This model postulates (i) a smooth oscillator (i.e., cellular clock), (ii) a slowly moving wavefront (i.e., of differentiated tissue), and (iii) rapid change at the front (i.e., cellular differentiation).[38,39]

Scheme 1b shows that we are extending the clock and wavefront framework from biological development to the programmable fabrication of a self-assembling hydrogel. Specifically, we are studying the pH-responsive aminopolysaccharide chitosan that can be induced to self-assemble into a hydrogel through a neutralization mechanism. Previous investigators have shown that the diffusion of OH^- ions (from NaOH solution)[40−42] can induce chitosan's self-assembly (i.e., gelation) and that interruptions in this gelation yield complex structures with boundaries separating segments (these have been referred to as multilayer or onion structures).[43,44] Previous studies have shown that electrical inputs can trigger

Received: October 10, 2017
Revised: December 13, 2017
Published: December 15, 2017

DOI: 10.1021/acs.biomac.7b01464
Biomacromolecules 2018, 19, 364–373

Scheme 1[a]

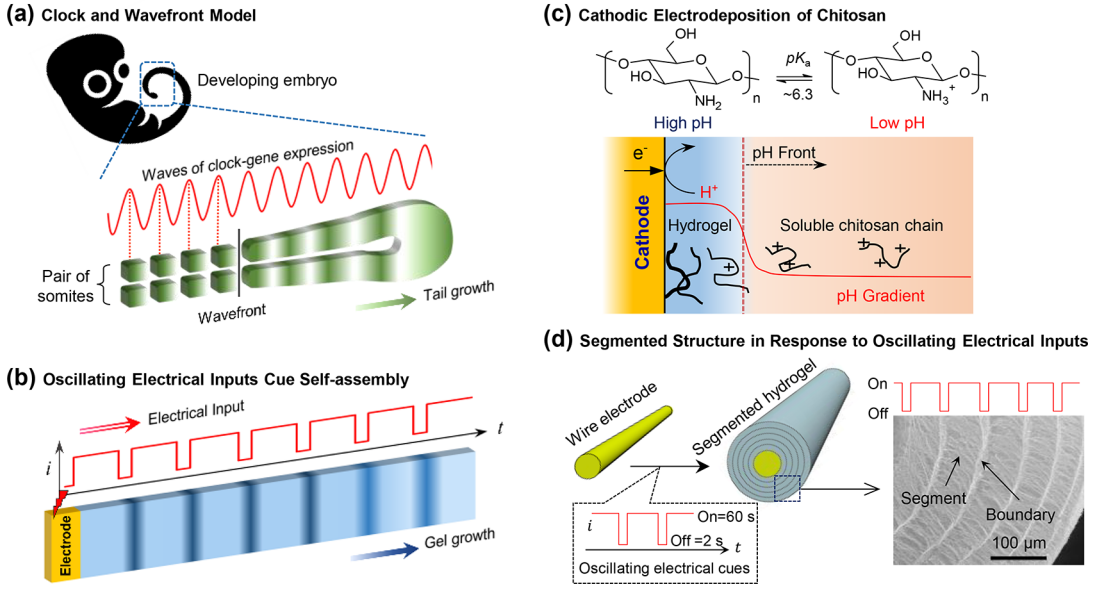

[a](a) Clock and wavefront model to explain the emergence of the segmented structure of embryonic somites. (b) Programmable fabrication of segmented hydrogel structure using oscillating electrical inputs to cue self-assembly. (c) Cathodic neutralization mechanism of chitosan's electrodeposition. (d) Segmented structure generated in response to oscillating electrical inputs. Adapted from ref 48 with permission from The Royal Society of Chemistry.

chitosan to electrodeposit at a cathode surface in response to the locally generated region of high pH,[45−47] and when oscillating electrical input signals are imposed a segmented structure emerges that has highly resolved boundaries generated within the hydrogel.[48] Several experimental observations of chitosan's electrodeposition are consistent with elements of the clock and wavefront model. First, during electrodeposition, a steep pH gradient separates the high-pH region adjacent to the electrode and the low-pH region in the bulk solution (Scheme 1c): This pH front grows slowly during the course of electrodeposition.[47] Second, the pH front colocalizes with the gelation front, consistent with a rapid change in structural organization from individual polysaccharide chains in solution to a 3D hydrogel network.[47] Finally, if the electrical input is imposed to oscillate with time, then a segmented spatial pattern emerges, as illustrated in Scheme 1d.[48]

Here we used all atom molecular modeling and in situ imaging through two novel methods (quantitative polarized light microscopy and Brillouin spectroscopy) to clarify the mechanisms responsible for the emergence of segmented structure during chitosan's electrodeposition. Furthermore, we show that a clock and wavefront model provide a reasonable framework to understand how temporally varying electrical input cues[49,50] can trigger the formation of spatial patterns. Specifically, we report that there are two components of the electrical input signal that control the emergence of the complex hydrogel structure. The electrical current is responsible for self-assembly because it is responsible for the electrochemical reactions that generate OH^-. The electrical potential (or field) is responsible for recruiting chains into the interface and appears to align these chains at the growing gel front. Oscillations in the electrical input create subtle changes in the relative importance of these two electrical components and can provide the program to guide self-assembly into deep free-energy wells that yield complex and spatially varying structure.

2. EXPERIMENTAL SECTION

2.1. Materials. Chitosan from crab shell (85% DA, ~200 kDa), fluorescein isothiocyanate-dextran (150 K), hydrogen peroxide (30%), and sodium chloride (99.5%) were purchased from Sigma-Aldrich. The deionized (DI) water was prepared from Millipore SUPER-Q water system with final resistivity >18 MΩ cm.

2.2. Electrodeposition. Chitosan solution (1% w/w) was prepared by adding chitosan powder into deionized water and slowly adding 1% hydrochloric acid to dissolve the chitosan. The final pH of the chitosan solution is ~5.5. The chitosan solution was filtered through a porous glass filter (~40 μm) to remove undissolved particles. Chitosan's electrodeposition was performed in the microfluidic channel device by filling the channel with a chitosan solution (1%, pH 5.5, 20 mM H_2O_2) with or without NaCl (0.4 M). The sidewall gold electrodes were connected to an electrochemical workstation (CHI6002E, CH Instrument, USA), and the "ON-OFF" input electrical signal sequence was programmed before initiating deposition. The working electrode was biased as cathode with a constant current density (typically 10−20 A/m^2), and a Pt wire was used as counter/reference electrode.

2.3. Instrumentation. Optical and fluorescence micrographs were obtained using an Olympus MVX10 MacroView microscope, and the images were analyzed using ImageJ (http://rsb.info.nih.gov/ij/). The morphology of the electrodeposited chitosan hydrogels was obtained using a scanning electron microscope (VEGA3 LMU, TESCAN) and crystallinity was measured with an X-ray diffraction apparatus (X'Pert Pro, PANalytical) with Cu Kα radiation source under the operating voltage of 40 kV and current of 20 mA. Quantitative polarized light microscopy (qPLM) was performed using a Meiji ML9730 polarized light microscope with 4× objective. The time-growth birefringence images were captured with attached 5 MP Lumenera Infinity 1−5 digital camera. The optical setup and computation of qPLM parameters have been previously described.[42,51−54] The details of the Brillouin microscopy setup were described elsewhere.[55] The microfluidic channel filled with chitosan solution was placed on the sample platform, and a laser beam for

DOI: 10.1021/acs.biomac.7b01464
Biomacromolecules 2018, 19, 364−373

Brillouin measurement was focused into the solution from the bottom side of the channel. The focused beam spot was about 0.5 × 0.5 × 2 μm. The light source was a single-mode 532 nm cw laser (Torus, LaserQuantum), and ~10 mW power was used in the measurement. For the in situ measurement, the laser beam was fixed at the position of 20 μm away from the cathode edge along gelation direction and 20 μm up from the bottom surface of the channel. For the scanning measurement, the channel was automatically moved back and forth repeatedly by the sample platform (Prior) along the gelation direction within the range of 300 μm. The scanning rate was set at 10 μm/s and the step size was 0.5 μm.

3. RESULTS

3.1. Modeling Evidence of the Role of Electrical Potential on Chain Migration. To examine the influence of the imposed electrical potential, we performed all-atom molecular dynamics simulations of a fully protonated chitosan chain composed of 20 glucosamine units in the presence of a uniform electric field of 0.004 V/nm without and with added 0.5 M salt. (Details of the simulation protocols are shown in the Supporting Information.) To reduce statistical uncertainties, simulation was repeated three times with electric field applied in x, y, or z directions. The simulated field strength was 1000 times greater than experiment to compensate for the 10^7 times shorter simulation time. As a control, three independent simulations in the absence of electric field were also conducted.

The control in Figure 1a shows that in the absence of an imposed field the calculated mean squared displacement (MSD) of the chain center of mass is small and increases nearly linearly with time. This is expected, because the motion of a chitosan chain in solution can be described by the equation for Brownian motion, MSD $\approx D\Delta\tau$, where D is the diffusion coefficient and $\Delta\tau$ is the elapsed time. In the presence of an imposed field, however, the MSD in the direction of the field is more than 10 times larger and increases nonlinearly with time. Fitting the data to MSD $\approx D\Delta\tau^{\alpha}$ returns α of ~1.1, suggestive of a superdiffusion behavior. This is because the charges on the chitosan chain experience the forces in the direction of the field, converting the normal diffusion process into an active transport (e.g., migration) process. With added salt, the force due to the electric field remains but is weakened due to the Debye–Hückel screening of the chitosan charges. As a result, the chain migration toward the electrode slows down but the nonlinear behavior persists.

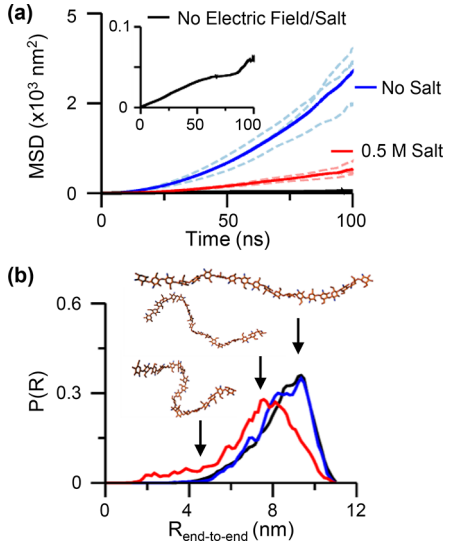

Figure 1. Electric field induces the protonated chitosan chains to migrate. (a) Mean squared displacement (MSD) of the chain as a function of elapsed time. The dashed lines represent the data from three independent runs. The solid lines represent the averages of the three runs. In the presence of electric field, only MSD in the direction of the field is plotted. The center of mass of the chain was used in the MSD calculation, with global displacement removed. The inset shows the MSD results in the absence of electric field or salt. For clarity, the average over the three runs in all three directions is shown. (b) Probability distribution of the end-to-end distance of the chain.

Next, we examined the chitosan chain dynamics by calculating the distribution of the end-to-end distance. Figure 1b shows that in the absence of salt the chain tends to be rigid with the most probable end-to-end distance (~9.5 nm) approaching the contour length (~11 nm)[56] and the imposed field having no obvious effect on the chain configurations. Interestingly, added salt increases the population of more flexible configurations. Our previous work revealed two underlying reasons.[56] First, the charges on the chitosan chain experience Debye–Hückel screening, which reduces the energetic penalty for the chain backbone bending. Second, salt disrupts the intramolecular hydrogen bonds that stabilize the extended backbone state. How salt affects the molecular structure of the chitosan gel state is not well understood. Because chitosan chains are more collapsed and flexible in the presence of salt, it may lead to less available sites for forming intermolecular hydrogen bonds.[56] However, our previous work also showed that salt destroys short-lived intermolecular hydrogen bonds during chitosan self-assembly, leading to the thermodynamically more favorable state with a larger number of intermolecular hydrogen bonds.[45] Dissecting salt effects on the structure and the formation of chitosan hydrogel is a continued effort.

3.2. Hydrogel Growth during the ON-Signal. The ON-signal is a constant user-defined direct current that induces the electrochemical proton-consuming reaction that leads to a high localized pH near the cathode surface. This pH shift triggers the stimuli-responsive aminopolysaccharide chitosan to self-assemble (i.e., electrodeposit) into a hydrogel through a neutralization mechanism.[45,47,57] During the ON-signal, a steep pH gradient emerges that separates the high-pH gel region adjacent to the electrode from the low-pH solution: This pH front grows slowly during the ON-signal and the growing pH front colocalizes with the gelation front consistent with a rapid change in structural organization from individual polysaccharide chains in solution to a 3D hydrogel network.[47]

To experimentally observe electrodeposition of the chitosan hydrogel, we used the fluidic device in Figure 2a, which is fabricated with sidewall electrodes and a transparent cover that allows real-time microscopic observation of film growth.[47] As schematically illustrated in Figure 2a, the two sidewalls for this fluidic device are fabricated from glass microscope slides that are each patterned with parallel 1 mm wide gold stripes using angled thermal evaporation with a shadow mask.[47] The fluidic channel was assembled by placing these 1 mm thick slides 1 mm apart and sandwiching these slides between two thin polydimethylsiloxane (PDMS) layers. (For clarity the top PDMS cover is not shown in Figure 2a.) Each sidewall electrode has an active area of 1 mm^2. The channel was filled with a chitosan solution and deposition was performed without fluid flow and with a constant ON-signal. The deposited hydrogel can span approximately half of the distance between

DOI: 10.1021/acs.biomac.7b01464
Biomacromolecules 2018, 19, 364–373

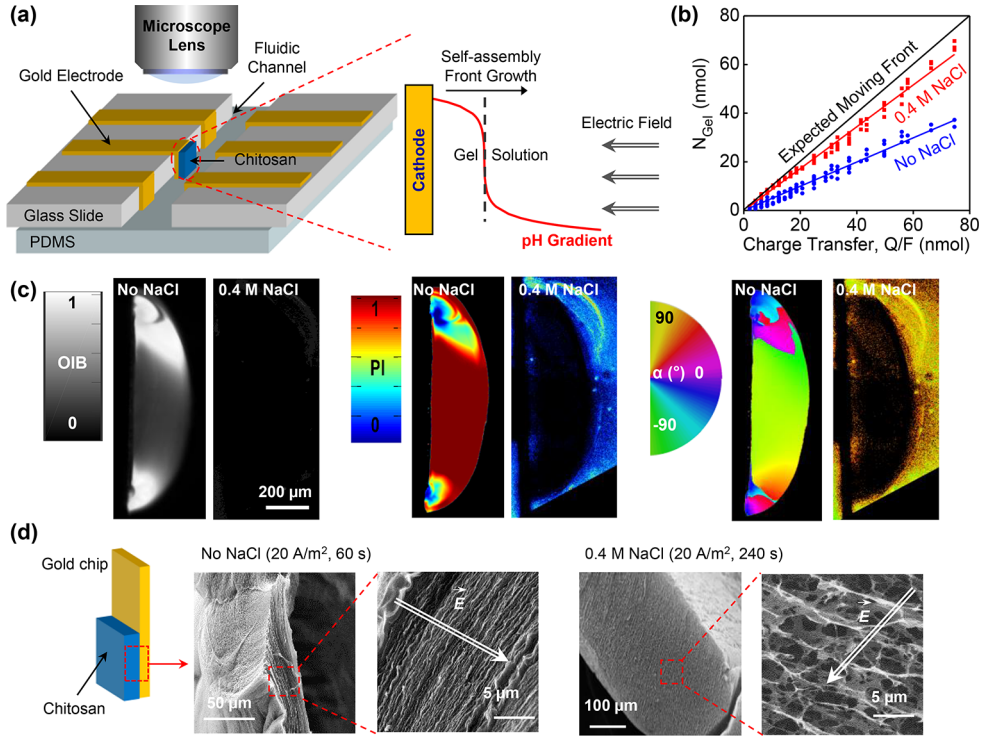

Figure 2. Emergence of structure during electrical ON-signal. (a) Schematics illustrating experimental device and the growing pH and self-assembly fronts due to the electrical current of the ON-signal. (b) Comparison of experimental results with expectations from a moving front model. (c) Quantitative polarized light microscopy (qPLM) metrics show the emergent microstructural organization: orientation-independent birefringence (OIB), parallelism index (PI), and local optical axis orientation (α). (d) SEM images of chitosan gel electrodeposited with a single ON-signal in the absence and presence of salt. Arrows indicate electric field.

the electrodes because of the competing pH gradients. (The high pH emanating from the cathode that is responsible for electrodeposition will merge with the low pH emanating from the anode.) A moving front model provides a semiquantitative macroscopic description of chitosan's electrodeposition.[48] (Details of the model are shown in the Supporting Information.) Chitosan's deposition in the absence or presence of salt is linear with time and increases with current density, which is qualitatively consistent with expectations from the moving front model (Figure S1). The rapid hydrogel growth observed in the presence of salt[58] shows reasonable quantitative agreement with expectations from the macroscopic moving front model, while greater deviation occurs for the slower growth observed in the absence of salt (Figure 2b). This deviation is consistent with the electric-field-inducing chitosan chains to migrate into the growing hydrogel. (The moving front model does not consider field-induced chain migration.) Independent experimental evidence of field-induced chitosan chain migration in the absence of salt during the ON-signal is shown in Figure S2 in the Supporting Information.

It may seem paradoxical that the growth speed of hydrogel in the presence of salt is faster than that in the absence of salt (Figure 2b), given that the MSD of chains in the presence of salt is smaller than that in the absence of salt (Figure 1a). The reason for this behavior is that gelation is induced by neutralization and the gel front grows faster when there are fewer chains to neutralize. If field-induced migration recruits more chains toward the cathode, then there are more chains to be neutralized for a given volume. (Under these conditions, the gels grow more slowly but have a higher chain density.)

Quantitative polarized light microscopy (qPLM)[42,51−54] was used to observe the emergence of microstructure during chitosan electrodeposition (Figure S3 in the Supporting Information). As expected, no birefringence is observed in the initial chitosan solution, indicating that this solution is optically isotropic. When chitosan is deposited in the absence of salt, the growing gels are observed to be birefringent with birefringence increasing over time, suggesting that the hydrogel chain density may be increasing (e.g., by syneresis) or chitosan chains may be reorganizing to yield greater alignment of chains with respect to each other. Minimal birefringence is observed in chitosan hydrogels deposited in the presence of salt.

In separate studies, gels were deposited and then maximum birefringence signal for each pixel was determined computationally from a series of raw birefringence images at different rotation angles of crossed polarizers and mapped as orientation-independent birefringence (OIB) (Figure 2c). Additional maps of parallelism index (PI) and local optical axis orientation (α) are also shown in Figure 2c. (Note: Strong edge effects are apparent in these maps and we focus analysis on the hydrogel adjacent to the central region of the electrode.) For deposition in the absence of salt, The high OIB observed suggests that these gels are organized into a highly anisotropic structure; the high PI indicates that these chains are highly aligned, and the local microstructural orientation indicates the polysaccharide chains are oriented parallel to the electrode surface. In contrast, the chitosan gels electrodeposited in the presence of salt possess very little birefringence, indicating an isotropic structure with no preferential chain alignment. (Note: The low birefringence for gels formed in the presence of salt prevents the

DOI: 10.1021/acs.biomac.7b01464
Biomacromolecules 2018, 19, 364−373

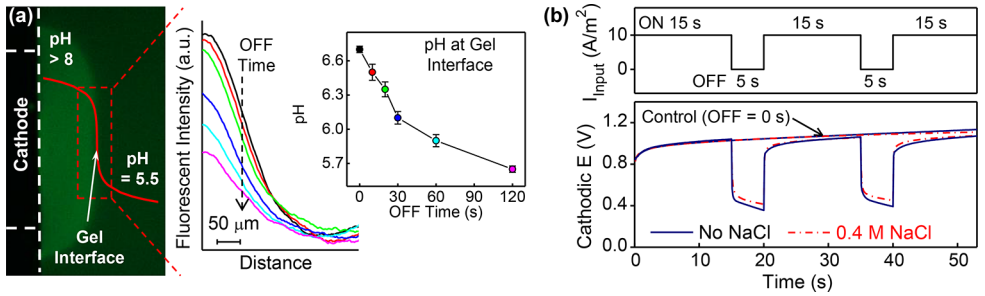

Figure 3. Dynamic relaxations during the electrical OFF-signal. (a) Dissipation of steep pH gradient at gel−solution interface when the electrical signal is switched from ON to OFF. Calibration curve of fluorescent intensity versus pH is shown in Figure S4b. (b) Rapid decrease in imposed cathodic potential when electrical signal is switched from ON to OFF, although a finite resting potential persists.

determination of meaningful PI or α values consistent with an isotropic microstructure.)

Additional evidence of chain alignment is provided by SEM images of electrodeposited hydrogels with a single ON-signal on a gold-coated surface. After chitosan's electrodeposition, the hydrogel film was rinsed with DI water, frozen in liquid nitrogen, and freeze-dried before SEM imaging. As shown in Figure 2d, the SEM images suggest that in the absence of salt chitosan chains are aligned parallel to the electrode surface, whereas in the presence of salt a less dense and less aligned structure is observed.

3.3. Relaxations during the OFF-Signal. One expectation during the OFF-signal (i = 0) is that the steep pH gradient established at the gel−solution interface will relax. To observe the spatiotemporal dissipation of this pH gradient we codeposited chitosan with FITC-dextran that provides pH-sensitive fluorescence.[59,60] After switching the electrical signal off, Figure 3a shows a gradual relaxation of the steep pH-gradient generated at the gel−solution interface (Figure S4). Partial relaxation of this pH front indicates that chitosan chains at/near the gel−solution interface should become progressively more protonated (i.e., charged). It should be noted that prolonged OFF time (e.g., 300 s) results in hydrogel's redissolving (Figure S4c).

In addition to a relaxation of the pH front, a switch from an ON-signal to an OFF-signal is expected to result in an instantaneous decrease in the cathodic potential imposed at the electrode surface. This is illustrated by the experiment in Figure 3b in which the ON-signal was interrupted by two brief OFF-signals and compared with a control with an uninterrupted ON-signal. The bottom panel of Figure 3b shows the expected decrease in cathodic potential when the electrical signal was switched OFF. Importantly, Figure 3b shows that there is a residual imposed resting potential of about −0.4 V during the electrical OFF-signal, and this resting potential exerts a sufficient electrical force to influence the chitosan chains (e.g., to drive migration) in the absence of salt (Figure S5).

3.4. Oscillating ON/OFF Signals To Create Segmented Hydrogel Structure. When chitosan hydrogels (with FITC-dextran) are deposited in response to oscillating ON-OFF signals segmented structures emerge as illustrated in Figure 4a. Segment growth occurs during the ON-signal while boundaries form during the OFF-signal. Segment growth and boundary formation are both sensitive to salt. In the absence of salt, the average thickness of the boundary increases with the duration of the OFF-signal, while the thickness of the boundary generated in the presence of salt is constant

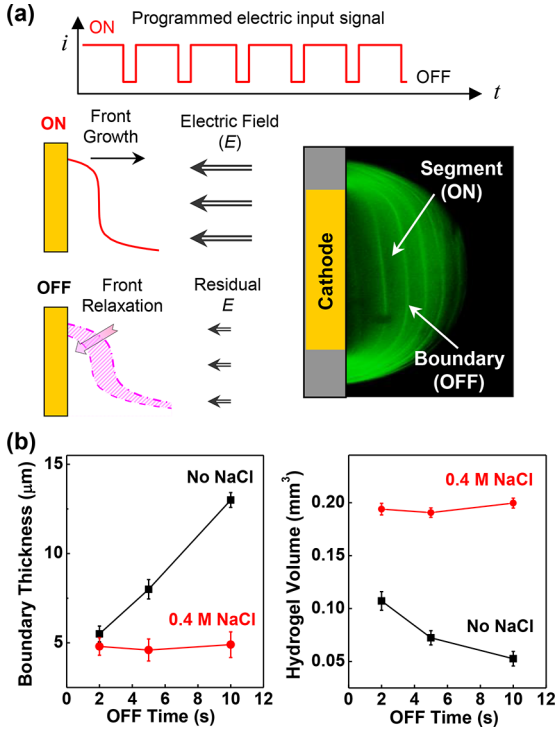

Figure 4. Boundary formation controlled by electrical OFF-signal. (a) Oscillating electrical ON/OFF-signals generate hydrogels with segment/boundary structure. (b) Boundary thickness and gel volume as a function of OFF-signal duration.

independent of OFF-signal duration (Figure 4b). These observations indicate that the residual electric field of the OFF-signal can recruit chitosan chains into the boundary, and this field-induced effect is abolished in the presence of salt.

To characterize the spatiotemporally varying properties of these segmented hydrogels, we coupled a Brillouin spectrometer with a confocal microscope. Brillouin spectroscopy uses the frequency shift of acoustically induced light scattering inside a sample to measure the high-frequency longitudinal modulus, which is correlated to the conventional Young's modulus.[55,61] We first applied Brillouin spectroscopy to detect chitosan gelation by focusing the laser in the fluidic channel 20 μm from the cathode, as illustrated in Figure 5a, and measuring the Brillouin frequency shift of the backward scattered light during the course of gelation. Figure 5a shows that when deposition was performed in the absence of salt, a distinct change in Brillouin shift (~0.02 GHz) is observed at the time that the gel front grew past the laser's position (150 s). When

DOI: 10.1021/acs.biomac.7b01464
Biomacromolecules 2018, 19, 364−373

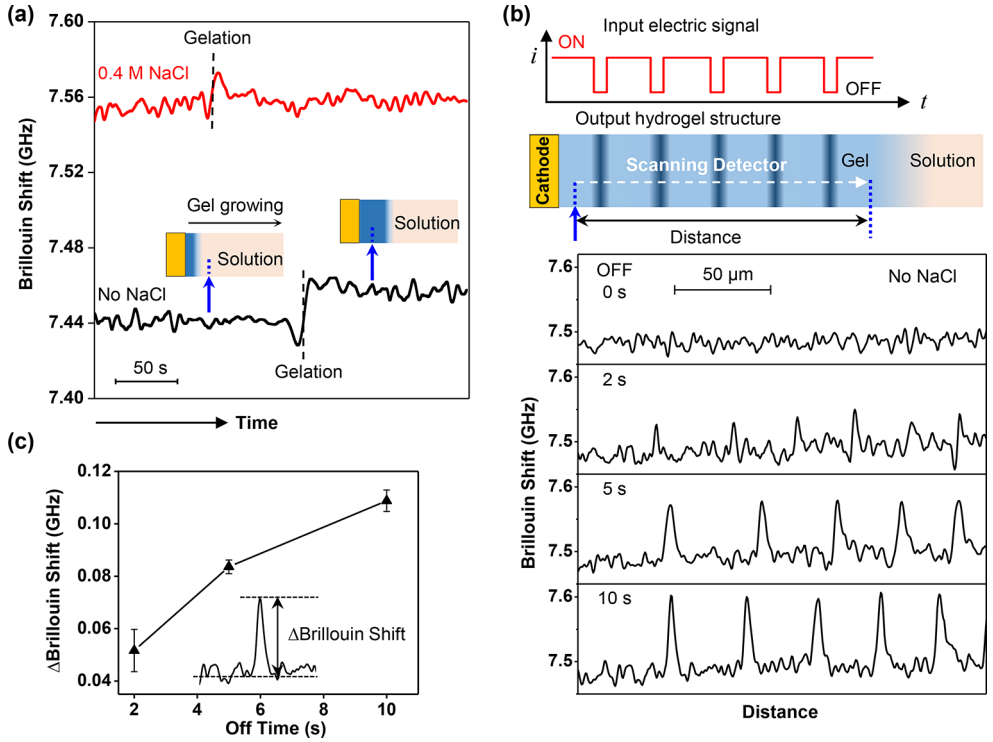

Figure 5. Brillouin spectroscopy shows: (a) Gelation in the absence of salt is readily detected (black curve), while gelation of weak gels formed in the presence of salt cannot be detected (red curve). (b) Stronger more defined boundaries are formed with longer OFF times. (c) Brillouin peak shift correlates to the duration of the OFF-signal.

the gel was grown in the presence of salt, the moment that the gel front passed the laser's position (100 s as observed by bright-field microscopy) could not be identified based on the Brillouin frequency shift. The inability to detect chitosan gelation in the presence of salt is consistent with previous observations that hydrogels deposited in the presence of high salt have very low moduli.[58]

In the subsequent experiment, we imposed oscillating electrical inputs and used Brillouin spectroscopy to observe segment growth and boundary formation in situ. Specifically, we used a chitosan solution lacking salt and imposed ON-signals of 30 s and OFF-signals of varying times. To monitor the real-time growth of the gel, we repeatedly scanned the Brillouin beam across the channel along the gelation direction (Figures S6 and S7). The upper curve in Figure 5b corresponds to a gel formed with a continuous ON-signal (0 s OFF-signal) and shows a flat baseline. The lower curves in Figure 5b show that distinct peaks are observed at the boundary regions that were generated during each OFF-signal, and these peak heights increased with OFF-signal duration, as shown in Figure 5c. Further tests showed that more complex sequences of ON/OFF signals could be imposed to generate hydrogels with more complex internal segment/boundary structural features (Figure S8). Together, these results indicate that the boundaries are regions of higher modulus and boundary modulus is controlled by OFF-signal duration in a field-dependent manner. The boundary regions have higher modulus presumably because the boundaries have greater chain density. During the OFF signal, there is a "relaxation" that occurs, allowing chain reorganization to form a denser interface. Mechanistically, we believe this relaxation involves a partial dissipation of the pH gradient, allowing the chains at the periphery to become protonated and partially mobile while the residual electrical field (associated with the resting potential shown in Figure 3b) still imposes a force to recruit chains into the interface and potentially also to align the chains at the interface.

3.5. Electrical Control of the Emerging Microstructure. The emerging structure generated in response to the oscillating electrical inputs is illustrated by the time-lapsed qPLM images of Figure 6a. These images show high birefringence in the segments formed during the ON-signal when deposition was performed in the absence of salt, while low birefringence is apparent in the segments generated in the presence of salt. A segmented hydrogel generated by oscillating electrical inputs in the absence of salt was further examined by generating parameter maps using qPLM. The orientation-independent birefringence (OIB) in Figure 6b shows a segmented appearance, and the segment regions have a high PI and are highly aligned. In addition, the local optical axis orientation (α) in Figure 6b indicates that the chitosan chains in the segments are aligned tangential to the direction of chitosan gel growth. These highly aligned regions of chitosan microstructure created during the ON-signal are separated by boundaries that appear to have higher chain density. The alignment of chitosan hydrogels in response to the oscillating electrical inputs is also illustrated by the SEM images of Figure 6c. Specifically, chitosan hydrogels were electrodeposited on a gold chip by imposing four cycles of ON and OFF signals. Aligned segments are observed for chitosan hydrogels deposited in the absence of salt, whereas gels deposited in the presence of salt show porous random structures. (Note: The hydrogel layers sometimes delaminate during freeze-drying, and this occurs for hydrogels prepared with or without salt.) Consistent with these microstructural differences, the

DOI: 10.1021/acs.biomac.7b01464
Biomacromolecules 2018, 19, 364−373

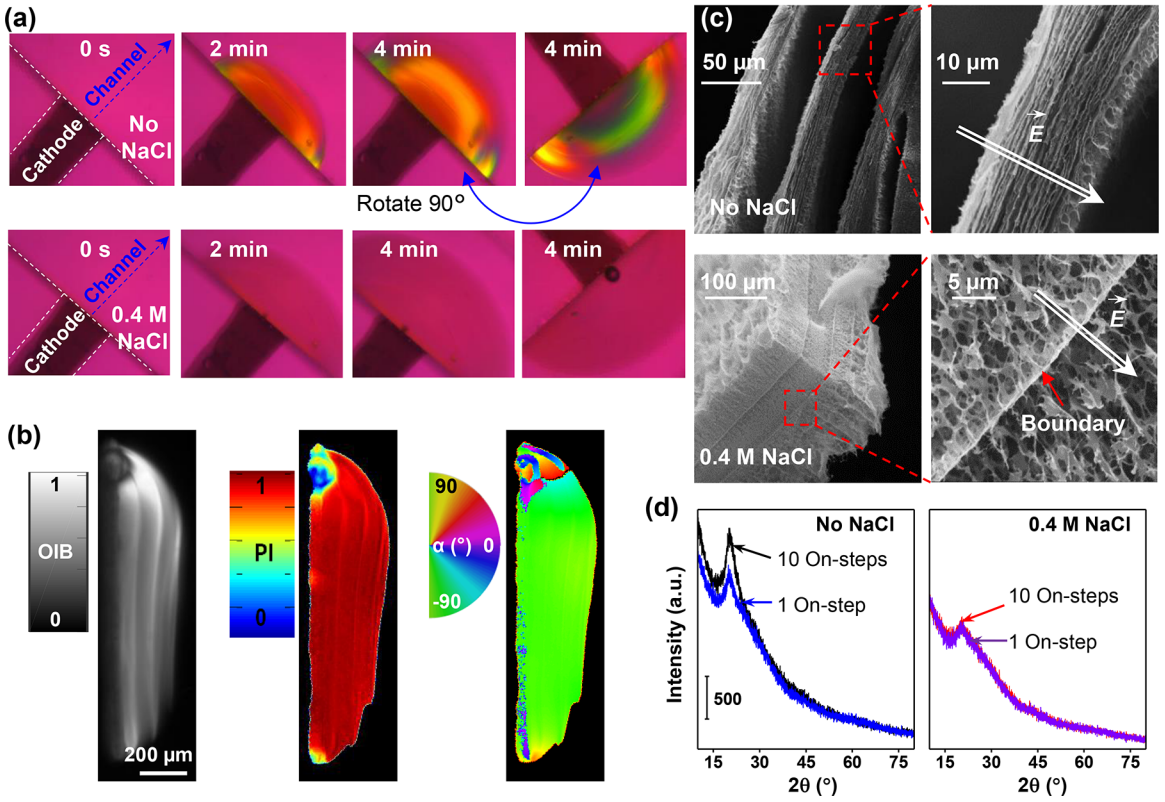

Figure 6. Electrical control of emerging microstructure. (a) Time-lapsed images show that gels deposited in the absence of NaCl are birefringent while gels deposited in the presence of NaCl (0.4 M) show little birefringence. (b) Quantitative polarized light microscopy metrics of orientation-independent birefringence (OIB), parallelism index (PI), and local optical axis orientation (α) of chitosan hydrogel electrodeposited in the absence of salt. (c) SEM images of segmented chitosan hydrogels show aligned segments for gels deposited in the absence of NaCl, while gels deposited in the presence of salt show porous random structures. Arrows indicate electric field. (d) XRD measurements suggest greater crystallinity for hydrogels electrodeposited in the absence of NaCl.

XRD results in Figure 6d indicate that greater crystallinity is observed for hydrogels electrodeposited in the absence of salt.

4. DISCUSSION

In this work, we studied the self-assembly of a stimuli-responsive polysaccharide and show that both the electrochemical and field components of an oscillating electrical input signal are integral to the emergence of segmented hydrogel patterns. Fundamentally, the energetics of self-organizing systems can vary between extremes of simple self-assembly toward a free-energy minimum and dissipative self-assembly that requires a continued input of energy.[62−67] Chitosan's electrodeposition is intermediate in that the electrical program guides assembly into deep free-energy wells (i.e., through strong noncovalent interactions)[45,68] that kinetically trap patterns that can persist indefinitely in the absence of continued energy inputs.[69−73] An intrinsic difference between programmed pattern formation in biological development and those generated by top-down electrofabrication involves the spatial supply of energy. In biology, the diffusing morphogens provide the cues, but the energy needed to execute a developmental program can be supplied locally by metabolism of the differentiating cells. In contrast with biology's distributed energy supply, the imposed electrical signals that cue hydrogel patterning must also provide the necessary energy for pattern development.

To elucidate the mechanisms of emergent segmented structure during chitosan's electrodeposition, we used a fluidic device with sidewall electrodes (Figure 2a) that allows real-time microscopic observation of hydrogel growth.[47] Importantly, the fluidic device allows us to apply two unconventional experimental methodologies to observe the in situ emergence of chitosan's structure during electrodeposition. Quantitative polarized light microscopy (qPLM)[42,51−54] revealed the anisotropic microstructural organization and chitosan chain alignment within the emerging hydrogel. Brillouin spectroscopy[55] showed that the temporally varying imposed electrical signals controlled the generation of spatially varying internal patterns and accompanying gradients in mechanical properties with high-modulus boundary regions separating the lower-modulus segments. By integrating the independent information obtained from these two novel experimental methods and augmenting this information with molecular dynamics simulations,[45,56] we are able to clarify the mechanisms responsible for the emergence of segmented structure during chitosan's electrodeposition. That is the imposed current induces electrochemical reactions that provide the pH cues that trigger self-assembly, while the imposed potential (i.e., field) provides the cues that recruit chains to the interface. Screening the electrical potential with salt during electrodeposition does not prevent self-assembly but yields weak gels with no obvious microstructural alignment.

The structural features (i.e., segments and boundaries) of our electrofabricated hydrogel films can be readily controlled by programming the duration of the ON- and OFF-signals. The feature size of the boundaries is in the micrometer range

DOI: 10.1021/acs.biomac.7b01464
Biomacromolecules 2018, 19, 364−373

(Figure 4b), which is smaller than the typical feature size (~200 μm) of hydrogels fabricated with current top-down methods such as 3D bioprinting.[74−76] In addition, the microstructural alignment of hydrogel film can also be easily tuned from anisotropic to nearly isotropic by varying salt content in deposition solution. Importantly, the hydrogel film fabricated by this electrical programming is mechanically and structurally heterogeneous (i.e., has alternating segments and boundaries) but chemically homogeneous (i.e., the patterning is achieved within a hydrogel composed of a single polysaccharide with no change in composition). This decoupling of structural properties from chemical composition should provide new capabilities for studies in mechanobiology and cell−cell communication.

5. CONCLUSIONS

Electrical signals can be imposed with exquisite temporal and quantitative precision, and this work illustrates how subtleties of these signals can be exploited to guide polysaccharide self-assembly into deep free energy wells that yield spatially varying kinetically stable structure. The imposed current induces electrochemical reactions that provide the pH cues that trigger self-assembly, while the imposed potential provides the cues that recruit chains to and aligns them at the interface. Screening the electrical potential with salt during electrodeposition does not prevent self-assembly but yields weak gels with no obvious microstructural alignment. Oscillating electrical inputs shift the balance of interactions, enabling segmented structures to be generated with boundary regions that are denser with higher modulus. The ability of programmable electrical inputs to provide the temporally varying cues for hydrogels to organize into complex spatial patterns is consistent with the clock and wavefront framework and indicates that top-down electrofabrication can organize soft matter with structural complexities approaching those of biology.

Biology often serves as the model illustrating how structure controls important functions. Structure is obviously integral to mechanical functions, and steep stiffness gradients are often required to satisfy dramatically different mechanical needs (e.g., a hard outer exoskeleton connected to a more compliant underlying soft tissue).[77−80] Advances in mechanobiology are also revealing that more subtle cellular responses (e.g., adhesion and spreading) are controlled by surface structure/properties, and these observations provide important criteria for the fabrication of tissue engineering scaffolds.[3,81−84] Biology also relies on dynamic structures that are constructed from reversible noncovalent interactions to perform important information processing functions. Classic examples of such dynamic structures include virus particles that disassemble and reassemble during the infection cycle and neurotransmitter vesicles that are important for localized molecular signaling between nerve cells. These latter examples provide insights into how to design nanoparticle systems for the storage, targeting, and delivery of therapeutics[85−87] and for the fabrication of self-healing and reconfigurable materials.[68,88,89] Results reported here suggest that electrofabrication offers advantages in comparison with alternative photolithographic or printing methods for hydrogel fabrication in that reversible (i.e., dynamic) structures can be programmed to assemble in response to external stimuli that can imposed with considerable spatiotemporal control. Furthermore, the complex chitosan structures generated in this study are achieved without a change in composition, and thus electrofabrication with this stimuli-responsive self-assembling polysaccharide allows a decoupling of hydrogel structure and composition. Finally, this work demonstrates the application of advanced methods (i.e., molecular modeling, qPLM and Brillouin spectroscopy) to characterize hierarchical structure of the fabricated hydrogels. Advances in soft matter characterization may be integral to enhancing our capabilities to create complex soft matter for a range of emerging applications.

■ ASSOCIATED CONTENT

Supporting Information

The Supporting Information is available free of charge on the ACS Publications website at DOI: 10.1021/acs.biomac.7b01464.

Molecular modeling, moving front model, and Supporting Figures S1−S8. (PDF)

■ AUTHOR INFORMATION

Corresponding Authors

*X.-W.S.: E-mail: shixwwhu@163.com.
*G.F.P.: E-mail: gpayne@umd.edu.

ORCID

Jana Shen: 0000-0002-3234-0769
Gregory F. Payne: 0000-0003-2566-4041

Present Address

#K.Y.: College of Materials Science and Engineering, Wuhan Textile University, Wuhan 430200, People's Republic of China.

Author Contributions

▽K.Y. and Y.L. contributed equally.

Notes

The authors declare no competing financial interest.

■ ACKNOWLEDGMENTS

This work has been supported by United States National Science Foundation (DMREF-1435957) and DTRA (HDTRA1-13-1-0037), National Natural Science Foundation of China (51373124, 21334005), Fundamental Research Funds for the Central Universities (2042016kf0145), Natural Science Foundation of Hubei Province of China (Team Project, No. 2015CFA017), and the China Scholarship Council.

■ REFERENCES

(1) Green, J. J.; Elisseeff, J. H. Mimicking Biological Functionality with Polymers for Biomedical Applications. *Nature* **2016**, *540*, 386−394.
(2) Slaughter, B. V.; Khurshid, S. S.; Fisher, O. Z.; Khademhosseini, A.; Peppas, N. A. Hydrogels in Regenerative Medicine. *Adv. Mater.* **2009**, *21*, 3307−3329.
(3) Li, Y. L.; Xiao, Y.; Liu, C. S. The Horizon of Materiobiology: A Perspective on Material-Guided Cell Behaviors and Tissue Engineering. *Chem. Rev.* **2017**, *117*, 4376−4421.
(4) Bajaj, P.; Schweller, R. M.; Khademhosseini, A.; West, J. L.; Bashir, R. 3D Biofabrication Strategies for Tissue Engineering and Regenerative Medicine. *Annu. Rev. Biomed. Eng.* **2014**, *16*, 247−276.
(5) Cui, H. T.; Nowicki, M.; Fisher, J. P.; Zhang, L. G. 3D Bioprinting for Organ Regeneration. *Adv. Healthcare Mater.* **2017**, *6*, 1601118.

(6) Guvendiren, M.; Molde, J.; Soares, R. M. D.; Kohn, J. Designing Biomaterials for 3D Printing. *ACS Biomater. Sci. Eng.* **2016**, *2*, 1679−1693.
(7) Zhu, W.; Ma, X. Y.; Gou, M. L.; Mei, D. Q.; Zhang, K.; Chen, S. C. 3D Printing of Functional Biomaterials for Tissue Engineering. *Curr. Opin. Biotechnol.* **2016**, *40*, 103−112.
(8) Jin, Y. F.; Liu, C. C.; Chai, W. X.; Compaan, A.; Huang, Y. Self-Supporting Nanoclay as Internal Scaffold Material for Direct Printing of Soft Hydrogel Composite Structures in Air. *ACS Appl. Mater. Interfaces* **2017**, *9*, 17456−17465.
(9) You, F.; Wu, X.; Zhu, N.; Lei, M.; Eames, B. F.; Chen, X. B. 3D Printing of Porous Cell-Laden Hydrogel Constructs for Potential Applications in Cartilage Tissue Engineering. *ACS Biomater. Sci. Eng.* **2016**, *2*, 1200−1210.
(10) Caliari, S. R.; Burdick, J. A. A Practical Guide to Hydrogels for Cell Culture. *Nat. Methods* **2016**, *13*, 405−414.
(11) Chaudhuri, O. Viscoelastic Hydrogels for 3D Cell Culture. *Biomater. Sci.* **2017**, *5*, 1480−1490.
(12) Chaudhuri, O.; Gu, L.; Klumpers, D.; Darnell, M.; Bencherif, S. A.; Weaver, J. C.; Huebsch, N.; Lee, H. P.; Lippens, E.; Duda, G. N.; Mooney, D. J. Hydrogels with Tunable Stress Relaxation Regulate Stem Cell Fate and Activity. *Nat. Mater.* **2015**, *15*, 326−334.
(13) Higuchi, A.; Ling, Q. D.; Chang, Y.; Hsu, S. T.; Umezawa, A. Physical Cues of Biomaterials Guide Stem Cell Differentiation Fate. *Chem. Rev.* **2013**, *113*, 3297−3328.
(14) Brandl, F.; Sommer, F.; Goepferich, A. Rational Design of Hydrogels for Tissue Engineering: Impact of Physical Factors on Cell Behavior. *Biomaterials* **2007**, *28*, 134−146.
(15) Fusco, S.; Panzetta, V.; Embrione, V.; Netti, P. A. Crosstalk Between Focal Adhesions and Material Mechanical Properties Governs Cell Mechanics and Functions. *Acta Biomater.* **2015**, *23*, 63−71.
(16) Loebel, C.; Szczesny, S. E.; Cosgrove, B. D.; Alini, M.; Zenobi-Wong, M.; Mauck, R. L.; Eglin, D. Cross-Linking Chemistry of Tyramine-Modified Hyaluronan Hydrogels Alters Mesenchymal Stem Cell Early Attachment and Behavior. *Biomacromolecules* **2017**, *18*, 855−864.
(17) Hachet, E.; Van Den Berghe, H.; Bayma, E.; Block, M. R.; Auzely-Velty, R. Design of Biomimetic Cell-Interactive Substrates Using Hyaluronic Acid Hydrogels with Tunable Mechanical Properties. *Biomacromolecules* **2012**, *13*, 1818−1827.
(18) Frank, V.; Kaufmann, S.; Wright, R.; Horn, P.; Yoshikawa, H. Y.; Wuchter, P.; Madsen, J.; Lewis, A. L.; Armes, S. P.; Ho, A. D.; Tanaka, M. Frequent Mechanical Stress Suppresses Proliferation of Mesenchymal Stem Cells from Human Bone Marrow without Loss of Multipotency. *Sci. Rep.* **2016**, *6*, 24264.
(19) Ren, K. X.; Cui, H. T.; Xu, Q. H.; He, C. L.; Li, G.; Chen, X. S. Injectable Polypeptide Hydrogels with Tunable Microenvironment for 3D Spreading and Chondrogenic Differentiation of Bone-Marrow-Derived Mesenchymal Stem Cells. *Biomacromolecules* **2016**, *17*, 3862−3871.
(20) Ye, K.; Cao, L. P.; Li, S. Y.; Yu, L.; Ding, J. D. Interplay of Matrix Stiffness and Cell-Cell Contact in Regulating Differentiation of Stem Cells. *ACS Appl. Mater. Interfaces* **2016**, *8*, 21903−21913.
(21) Jeffords, M. E.; Wu, J. L.; Shah, M.; Hong, Y.; Zhang, G. Tailoring Material Properties of Cardiac Matrix Hydrogels To Induce Endothelial Differentiation of Human Mesenchymal Stem Cells. *ACS Appl. Mater. Interfaces* **2015**, *7*, 11053−11061.
(22) Gao, M.; Zheng, H. Z.; Ren, Y.; Lou, R. Y.; Wu, F.; Yu, W. T.; Liu, X. D.; Ma, X. J. A Crucial role for Spatial Distribution in Bacterial Quorum Sensing. *Sci. Rep.* **2016**, *6*, 34695.
(23) Flickinger, S. T.; Copeland, M. F.; Downes, E. M.; Braasch, A. T.; Tuson, H. H.; Eun, Y. J.; Weibel, D. B. Quorum Sensing between Pseudomonas aeruginosa Biofilms Accelerates Cell Growth. *J. Am. Chem. Soc.* **2011**, *133*, 5966−5975.
(24) Geckil, H.; Xu, F.; Zhang, X. H.; Moon, S.; Demirci, U. Engineering Hydrogels as Extracellular Matrix Mimics. *Nanomedicine* **2010**, *5*, 469−484.
(25) Gines, G.; Zadorin, A. S.; Galas, J.-C.; Fujii, T.; Estevez-Torres, A.; Rondelez, Y. Microscopic Agents Programmed by DNA Circuits. *Nat. Nanotechnol.* **2017**, *12*, 351−359.
(26) Zadorin, A. S.; Rondelez, Y.; Galas, J. C.; Estevez-Torres, A. Synthesis of Programmable Reaction-Diffusion Fronts Using DNA Catalyzers. *Phys. Rev. Lett.* **2015**, *114*, 068301.
(27) Purvis, J. E.; Lahav, G. Encoding and Decoding Cellular Information through Signaling Dynamics. *Cell* **2013**, *152*, 945−956.
(28) Beaupeux, M.; Francois, P. Positional Information from Oscillatory Phase shifts: Insights from In Silico Evolution. *Phys. Biol.* **2016**, *13*, 036009.
(29) Turing, A. M. The Chemical Basis of Morphogenesis. *Philos. Trans. R. Soc., B* **1952**, *237*, 37−72.
(30) Tompkins, N.; Li, N.; Girabawe, C.; Heymann, M.; Ermentrout, G. B.; Epstein, I. R.; Fraden, S. Testing Turing's Theory of Morphogenesis in Chemical Cells. *Proc. Natl. Acad. Sci. U. S. A.* **2014**, *111*, 4397−4402.
(31) Yabe, T.; Takada, S. Molecular Mechanism for Cyclic Generation of Somites: Lessons from Mice and Zebrafish. *Dev. Growth Diff.* **2016**, *58*, 31−42.
(32) Signon, L.; Nowakowski, B.; Lemarchand, A. Modeling Somite Scaling in Small Embryos in the Framework of Turing Patterns. *Phys. Rev. E: Stat. Phys., Plasmas, Fluids, Relat. Interdiscip. Top.* **2016**, *93*, 042402.
(33) Dziekan, P.; Nowakowski, B.; Lemarchand, A. Reaction-Diffusion Scheme for the Clock and Wavefront Mechanism of Pattern Formation. *Eur. Phys. J. B* **2014**, *87*, 77.
(34) Murray, P. J.; Maini, P. K.; Baker, R. E. The Cock and Wavefront Model Revisited. *J. Theor. Biol.* **2011**, *283*, 227−238.
(35) Kondo, S.; Miura, T. Reaction-Diffusion Model as a Framework for Understanding Biological Pattern Formation. *Science* **2010**, *329*, 1616−1620.
(36) Vonk, F. J.; Richardson, M. K. Developmental Biology - Serpent Clocks Tick Faster. *Nature* **2008**, *454*, 282−283.
(37) Gomez, C.; Ozbudak, E. M.; Wunderlich, J.; Baumann, D.; Lewis, J.; Pourquie, O. Control of Segment Number in Vertebrate Embryos. *Nature* **2008**, *454*, 335−339.
(38) Dias, A. S.; de Almeida, I.; Belmonte, J. M.; Glazier, J. A.; Stern, C. D. Somites Without a Clock. *Science* **2014**, *343*, 791−795.
(39) Cooke, J.; Zeeman, E. C. Clock and Wavefront Model for Control of Number of Repeated Structures during Animal Morphogenesis. *J. Theor. Biol.* **1976**, *58*, 455−476.
(40) Dobashi, T.; Tomita, N.; Maki, Y.; Chang, C. P.; Yamamoto, T. An Analysis of Anisotropic Gel Forming Process of Chitosan. *Carbohydr. Polym.* **2011**, *84*, 709−712.
(41) Nie, J. Y.; Lu, W. T.; Ma, J. J.; Yang, L.; Wang, Z. K.; Qin, A.; Hu, Q. L. Orientation in Multi-layer Chitosan Hydrogel: Morphology, Mechanism, and Design Principle. *Sci. Rep.* **2015**, *5*, 7635.
(42) Maki, Y.; Furusawa, K.; Yasuraoka, S.; Okamura, H.; Hosoya, N.; Sunaga, M.; Dobashi, T.; Sugimoto, Y.; Wakabayashi, K. Universality and Specificity in Molecular Orientation in Anisotropic Gels Prepared by Diffusion Method. *Carbohydr. Polym.* **2014**, *108*, 118−126.
(43) Ladet, S. G.; Tahiri, K.; Montembault, A. S.; Domard, A. J.; Corvol, M. T. M. Multi-membrane Chitosan Hydrogels as Chondrocytic Cell Bioreactors. *Biomaterials* **2011**, *32*, 5354−5364.
(44) Ladet, S.; David, L.; Domard, A. Multi-membrane Hydrogels. *Nature* **2008**, *452*, 76−79.
(45) Morrow, B. H.; Payne, G. F.; Shen, J. pH-Responsive Self-Assembly of Polysaccharide through a Rugged Energy Landscape. *J. Am. Chem. Soc.* **2015**, *137*, 13024−13030.
(46) Liu, Y.; Kim, E.; Ghodssi, R.; Rubloff, G. W.; Culver, J. N.; Bentley, W. E.; Payne, G. F. Biofabrication to Build the Biology-device Interface. *Biofabrication* **2010**, *2*, 022002.
(47) Cheng, Y.; Luo, X. L.; Betz, J.; Buckhout-White, S.; Bekdash, O.; Payne, G. F.; Bentley, W. E.; Rubloff, G. W. In Situ Quantitative Visualization and Characterization of Chitosan Electrodeposition with Paired Sidewall Electrodes. *Soft Matter* **2010**, *6*, 3177−3183.

DOI: 10.1021/acs.biomac.7b01464
Biomacromolecules 2018, 19, 364−373

(48) Yan, K.; Ding, F. Y.; Bentley, W. E.; Deng, H. B.; Du, Y. M.; Payne, G. F.; Shi, X. W. Coding for Hydrogel Organization through Signal Guided Self-assembly. *Soft Matter* **2014**, *10*, 465−469.
(49) Tu, Y. F.; Peng, F.; Adawy, A.; Men, Y. J.; Abdelmohsen, L.; Wilson, D. A. Mimicking the Cell: Bio-Inspired Functions of Supramolecular Assemblies. *Chem. Rev.* **2016**, *116*, 2023−2078.
(50) Velichko, Y. S.; Mantei, J. R.; Bitton, R.; Carvajal, D.; Shull, K. R.; Stupp, S. I. Electric Field Controlled Self-Assembly of Hierarchically Ordered Membranes. *Adv. Funct. Mater.* **2012**, *22*, 369−377.
(51) Raub, C. B.; Hsu, S. C.; Chan, E. F.; Shirazi, R.; Chen, A. C.; Chnari, E.; Semler, E. J.; Sah, R. L. Microstructural Remodeling of Articular Cartilage Following Defect Repair by Osteochondral Autograft Transfer. *Osteoarthritis Cartilage* **2013**, *21*, 860−868.
(52) Kocsis, K.; Hyttinen, M.; Helminen, H. J.; Aydelotte, M. B.; Modis, L. Combination of Digital Image Analysis and Polarization Microscopy: Theoretical Considerations and Experimental Data. *Microsc. Res. Tech.* **1998**, *43*, 511−517.
(53) Li, K.; Correa, S. O.; Pham, P.; Raub, C. B.; Luo, X. Birefringence of Flow-assembled Chitosan Membranes in Microfluidics. *Biofabrication* **2017**, *9*, 034101.
(54) Rieppo, J.; Hallikainen, J.; Jurvelin, J. S.; Kiviranta, I.; Helminen, H. J.; Hyttinen, M. M. Practical Considerations in the Use of Polarized Light Microscopy in the Analysis of the Collagen Network in Articular Cartilage. *Microsc. Res. Tech.* **2008**, *71*, 279−287.
(55) Scarcelli, G.; Polacheck, W. J.; Nia, H. T.; Patel, K.; Grodzinsky, A. J.; Kamm, R. D.; Yun, S. H. Noncontact Three-Dimensional Mapping of Intracellular Hydromechanical Properties by Brillouin Microscopy. *Nat. Methods* **2015**, *12*, 1132−1134.
(56) Tsai, C.-C.; Morrow, B. H.; Chen, W.; Payne, G. F.; Shen, J. Toward Understanding the Environmental Control of Hydrogel Film Properties: How Salt Modulates the Flexibility of Chitosan Chains. *Macromolecules* **2017**, *50*, 5946−5952.
(57) Simchi, A.; Pishbin, F.; Boccaccini, A. R. Electrophoretic Deposition of Chitosan. *Mater. Lett.* **2009**, *63*, 2253−2256.
(58) Liu, Y.; Zhang, B.; Gray, K. M.; Cheng, Y.; Kim, E.; Rubloff, G. W.; Bentley, W. E.; Wang, Q.; Payne, G. F. Electrodeposition of A Weak Polyelectrolyte Hydrogel: Remarkable Effects of Salt on Kinetics, Structure and Properties. *Soft Matter* **2013**, *9*, 2703−2710.
(59) Chauhan, V. M.; Burnett, G. R.; Aylott, J. W. Dual-Fluorophore Ratiometric pH Nanosensor with Tuneable pK(a) and Extended Dynamic Range. *Analyst* **2011**, *136*, 1799−1801.
(60) Liu, Y. H.; Dam, T. H.; Pantano, P. A pH-sensitive Nanotip Array Imaging Sensor. *Anal. Chim. Acta* **2000**, *419*, 215−225.
(61) Scarcelli, G.; Kim, P.; Yun, S. H. In Vivo Measurement of Age-Related Stiffening in the Crystalline Lens by Brillouin Optical Microscopy. *Biophys. J.* **2011**, *101*, 1539−1545.
(62) Maiti, S.; Fortunati, I.; Ferrante, C.; Scrimin, P.; Prins, L. J. Dissipative Self-assembly of Vesicular Nanoreactors. *Nat. Chem.* **2016**, *8*, 725−731.
(63) Epstein, I. R.; Xu, B. Reaction-Diffusion Processes at the Nano- and Microscales. *Nat. Nanotechnol.* **2016**, *11*, 312−319.
(64) Mattia, E.; Otto, S. Supramolecular Systems Chemistry. *Nat. Nanotechnol.* **2015**, *10*, 111−119.
(65) Heuser, T.; Steppert, A. K.; Lopez, C. M.; Zhu, B. L.; Walther, A. Generic Concept to Program the Time Domain of Self-Assemblies with a Self-Regulation Mechanism. *Nano Lett.* **2015**, *15*, 2213−2219.
(66) England, J. L. Dissipative Adaptation in Driven Self-assembly. *Nat. Nanotechnol.* **2015**, *10*, 919−923.
(67) Karsenti, E. Self-Organization in Cell Biology: A Brief History. *Nat. Rev. Mol. Cell Biol.* **2008**, *9*, 255−262.
(68) He, H.; Cao, X.; Dong, H.; Ma, T.; Payne, G. F. Reversible Programing of Soft Matter with Reconfigurable Mechanical Properties. *Adv. Funct. Mater.* **2017**, *27*, 1605665.
(69) Stupp, S. I.; Zha, R. H.; Palmer, L. C.; Cui, H. G.; Bitton, R. Self-assembly of Biomolecular Soft Matter. *Faraday Discuss.* **2013**, *166*, 9−30.
(70) Zhang, J.; Li, X.; Li, X. Stimuli-triggered Structural Engineering of Synthetic and Biological Polymeric Assemblies. *Prog. Polym. Sci.* **2012**, *37*, 1130−1176.
(71) Rybtchinski, B. Adaptive Supramolecular Nanomaterials Based on Strong Noncovalent Interactions. *ACS Nano* **2011**, *5*, 6791−6818.
(72) Moore, J. S.; Kraft, M. L. Chemistry - Synchronized Self-assembly. *Science* **2008**, *320*, 620−621.
(73) Capito, R. M.; Azevedo, H. S.; Velichko, Y. S.; Mata, A.; Stupp, S. I. Self-assembly of Large and Small Molecules into Hierarchically Ordered Sacs and Membranes. *Science* **2008**, *319*, 1812−1816.
(74) Duan, B.; Hockaday, L. A.; Kang, K. H.; Butcher, J. T. 3D Bioprinting of Heterogeneous Aortic Valve Conduits with Alginate/Gelatin Hydrogels. *J. Biomed. Mater. Res., Part A* **2013**, *101A*, 1255−1264.
(75) Shang, W. F.; Liu, Y. T.; Wan, W. F.; Hu, C. Z.; Liu, Z. Y.; Wong, C. T.; Fukuda, T.; Shen, Y. J. Hybrid 3D Printing and Electrodeposition Approach for Controllable 3D Alginate Hydrogel Formation. *Biofabrication* **2017**, *9*, 025032.
(76) Xu, T.; Zhao, W. X.; Zhu, J. M.; Albanna, M. Z.; Yoo, J. J.; Atala, A. Complex Heterogeneous Tissue Constructs Containing Multiple Cell Types Prepared by Inkjet Printing Technology. *Biomaterials* **2013**, *34*, 130−139.
(77) Tadayon, M.; Amini, S.; Masic, A.; Miserez, A. The Mantis Shrimp Saddle: A Biological Spring Combining Stiffness and Flexibility. *Adv. Funct. Mater.* **2015**, *25*, 6437−6447.
(78) Weaver, J. C.; Milliron, G. W.; Miserez, A.; Evans-Lutterodt, K.; Herrera, S.; Gallana, I.; Mershon, W. J.; Swanson, B.; Zavattieri, P.; DiMasi, E.; Kisailus, D. The Stomatopod Dactyl Club: A Formidable Damage-Tolerant Biological Hammer. *Science* **2012**, *336*, 1275−1280.
(79) Miserez, A.; Schneberk, T.; Sun, C. J.; Zok, F. W.; Waite, J. H. The Transition from Stiff to Compliant Materials in Squid Beaks. *Science* **2008**, *319*, 1816−1819.
(80) Miserez, A.; Li, Y. L.; Waite, J. H.; Zok, F. Jumbo Squid Beaks: Inspiration for Design of Robust Organic Composites. *Acta Biomater.* **2007**, *3*, 139−149.
(81) Fan, X. L.; Zhu, L.; Wang, K.; Wang, B. J.; Wu, Y. Z.; Xie, W.; Huang, C. Y.; Chan, B. P.; Du, Y. N. Stiffness-Controlled Thermoresponsive Hydrogels for Cell Harvesting with Sustained Mechanical Memory. *Adv. Healthcare Mater.* **2017**, *6*, 1601152.
(82) Ivanovska, I. L.; Shin, J. W.; Swift, J.; Discher, D. E. Stem Cell Mechanobiology: Diverse Lessons from Bone Marrow. *Trends Cell Biol.* **2015**, *25*, 523−532.
(83) Pedersen, J. A.; Swartz, M. A. Mechanobiology in the Third Dimension. *Ann. Biomed. Eng.* **2005**, *33*, 1469−1490.
(84) Discher, D. E.; Janmey, P.; Wang, Y. L. Tissue Cells Feel and Respond to the Stiffness of Their Substrate. *Science* **2005**, *310*, 1139−1143.
(85) Li, J. Y.; Qu, X.; Payne, G. F.; Zhang, C.; Zhang, Y. X.; Li, J. B.; Ren, J.; Hong, H.; Liu, C. S. Biospecific Self-Assembly of a Nanoparticle Coating for Targeted and Stimuli-Responsive Drug Delivery. *Adv. Funct. Mater.* **2015**, *25*, 1404−1417.
(86) Zhang, C.; Qu, X.; Li, J.; Hong, H.; Li, J.; Ren, J.; Payne, G. F.; Liu, C. Biofabricated Nanoparticle Coating for Liver-Cell Targeting. *Adv. Healthcare Mater.* **2015**, *4*, 1972−1981.
(87) Ding, B. S.; Dziubla, T.; Shuvaev, V. V.; Muro, S.; Muzykantov, V. R. Advanced Drug Delivery Systems That Target the Vascular Endothelium. *Mol. Interventions* **2006**, *6*, 98−112.
(88) Zhong, M.; Liu, X. Y.; Shi, F. K.; Zhang, L. Q.; Wang, X. P.; Cheetham, A. G.; Cui, H. G.; Xie, X. M. Self-healable, Tough and Highly Stretchable Ionic Nanocomposite Physical Hydrogels. *Soft Matter* **2015**, *11*, 4235−4241.
(89) Frei, R.; McWilliam, R.; Derrick, B.; Purvis, A.; Tiwari, A.; Di Marzo Serugendo, G. Self-healing and Self-repairing Technologies. *Int. J. Adv. Manuf. Technol.* **2013**, *69*, 1033−1061.

DOI: 10.1021/acs.biomac.7b01464
Biomacromolecules 2018, 19, 364−373